Pergamon

Planet. Space Sci., Vol. 44, No. 9, pp. 901–908, 1996

0032-0633/96 $15.00+0.00

0032-0633(95)00119-0

Measurements of ejection velocities in collisional disruption of ice spheres

Masahiko Arakawa and Michiya Higa

Institute of Low Temperature Science, Hokkaido University, Kita-ku Kita-19 Nishi-8, Sapporo 060, Japan

Received 28 April 1995; revised 4 September 1995; accepted 4 September 1995

Abstract. Impact experiments are performed on ice spheres to measure the velocity field of ejected ice fragments and the conditions under which the fragments would reaccumulate during accretion in the outer solar system are considered. A single-stage light gas gun set in a cold room at $-18°C$ and an image-converter camera running at $2\times10^5-1\times10^4$ frames per second with a xenon flash lamp are used for observing the collisional phenomena. Spherical projectiles of ice ($m_p = 1.5$ g) collide head-on with spherical targets ($M_t = 1.5$, 12, 172 g) at 150–690 m s^{-1}. The ejection velocity is observed to vary with the initial position and ranges from 3 to 1/10 of the impact velocity (V_i). The ejection velocity of fragments at the rear side of the target (V_e) varies with distance from the impact point according to a power law relation, $V_e = V_a(l/D)^{-n}$, where V_a is the antipodal velocity, l and D are the distance and the target diameter, and $n = 1.5$–2.0. V_a depends on the specific energy (Q) at a constant mass ratio ($m_p/M_t = 0.13$) and the empirical dependence is written as $V_a = 0.35\times Q^{0.52}$. The ejection velocity of fine fragments formed by the jetting process near the impact point is determined to be 1.7–2.9 times as large as the impact velocity irrespective of the target size and the impact velocity.

Introduction

Since planetary explorations by the *Voyager* spacecraft, volatile materials such as water ice have been recognized to be the main constituent minerals of icy satellites in the outer solar system. Thus, when we consider the growth process of the icy satellites in that region, it is necessary to study the physics of collisions among icy planetesimals. The velocity field of impact fragments is one of the most important physical properties of these collisional processes. When two bodies collide at high velocity, they fracture and many of the fragments are formed by an intensive shock wave and are ejected from the bodies. Fragments with velocities lower than the escape velocity of a body can be captured and contribute to its growth. Thus, the velocity distribution of the fragments is necessary to clarify the planetary growth process quantitatively.

The velocity fields of impact fragments of basalt and alumina targets were measured by Nakamura and Fujiwara (1991). They performed collisional experiments at high velocity (≥ 3 km s^{-1}) and obtained the three-dimensional velocity fields of fragments for collisional disruption that resulted in a large core fragment. Giblin *et al.* (1994) made fragmentation experiments on artificial rock by using explosives instead of the kinetic energy of the projectile and measured the velocity field of the fragments. These results were compared with a semi-empirical model of catastrophic disruption proposed by Paolicchi *et al.* (1989). However, the kinematic aspects of ice collisions have not been studied except for cratering by tiny projectiles (≤ 0.1 mm) (Frisch, 1991).

Numerical simulations of collisional disruption were performed with high time resolution by Asphaug and Melosh (1993) and Benz and Asphaug (1994). They developed a numerical model with an appropriate fracture criterion to obtain the mass distribution and the velocity field of fragments. In these simulations, the validity must be checked by comparing with real collisional phenomena in the laboratory. But, there is currently little information on the velocity field of collisional fragments for comparison.

Thus, we experimentally investigated the velocity field of ice fragments in catastrophic disruption in ice-on-ice collisions and considered the conditions for reaccumulation of icy planetesimals by means of an empirical relation derived from the experiments.

Experimental method

Impact experiments were made by using a single-stage vertical light gas gun set up in a cold room at Inst. Low

Correspondence to: M. Arakawa

Table 1. Experimental results on velocity measurements

Run No.	m_p (g)	M_t (g)	m_p/M_t	V_i (m s^{-1})	V_a (m s^{-1})	V_{jet} (m s^{-1})	V_{jet}/V_t
Run 1	1.59	12.5	0.13	153	—	408	2.7
Run 2	1.53	12.0	0.13	246	27.8	458	1.9
Run 3	1.54	12.0	0.13	333	25.5	909	2.7
Run 4	1.41	12.3	0.11	470	48.3	—	—
Run 5	1.51	12.3	0.12	575	54.5	1670	2.9
Run 6	1.51	11.3	0.14	687	73.5	1310	1.9
Run 7	1.39	1.57	0.89	480	—	826	1.7
Run 8	1.56	172	0.0091	495	—	1400	2.8

m_p and M_t are projectile mass and target mass. V_i, V_a, and V_{jet} are impact velocity, antipodal velocity, and jetting velocity, respectively.

Temp. Sci., Hokkaido Univ. (Kato *et al.*, 1995). The ambient temperature of the cold room is -18°C. The light gas gun uses high-pressure helium gas to accelerate an ice projectile set in the entrance of the gun barrel. The projectile was launched through the 1 m barrel at velocities between 150 and 690 m s^{-1} (Table 1) to a target in a vacuum chamber. The projectiles and the targets were spheres made of polycrystalline ice without visible pores. The ice projectiles were 15 mm in diameter and 1.5 g in mass (m_p), and the targets were 15, 30, and 71 mm in diameter and 1.5, 12, and 172 g in mass (M_t), respectively. The mass ratio of the projectile to the target is an important parameter for a collision and ranged from 0.89 to 0.0091 in these experiments. The spherical target was suspended with strings in the center of a transparent acrylic box ($20 \times 20 \times 20$ cm) positioned in the vacuum chamber.

Collisions were observed by a high speed image recording system. This system consisted of an image-converter camera (ULTRA NAC) and a xenon flash lamp with concave mirrors (15 cm) for a shadow photograph lighting system. The camera and the flash lamp were triggered when the projectile cut a laser beam installed just above the target. Still images of the high velocity ejecta were successfully taken by the system because of the short exposure time of the camera (700 ns). The brightness of the flash lamp and the lighting duration were strong (50 J) enough for our short exposure times and long (1 ms) enough for our recording time ($\leqslant 400$ μs), respectively. The camera view and the lighting direction were perpendicular to the impact axis and a head-on collision between the projectile and the target hanging freely in the acrylic box was intended for all experiments. Thus, a recorded two-dimensional image observed from one side can be interpreted as a three-dimensional one because of the presumed axial symmetry of the collision. The target was set between the camera and the flash lamp to obscure the light. When lighted from the back side, the target appeared as a black shadow in the recorded images. The camera can take 12 successive images at a speed of $2 \times 10^5 - 1 \times 10^4$ frames s^{-1} and can change the time interval between frames arbitrarily. This recording system enables us to measure the ejection velocity of ice fragments travelling faster than 1 km s^{-1} with sufficient accuracy.

Experimental results

Figure 1 shows snap shots of the collision taken by the high speed camera (Run 6, impact velocity (V_i) of 687 m s^{-1} and mass ratio (m_p/M_t) of 0.14). The time of the first image is set at 0 μs and the time relative to the first image is labeled in each image. Two black circular regions in the first image are the projectile and the target: the upper cap surface and the lower sphere are the projectile and the target, respectively. Note that high velocity fragments are ejected horizontally from the impact point. These fragments expand symmetrically toward both sides and grow with time to make a wing-like form. The maximum velocity of this expanding wing-like form is about 1.3 km s^{-1}, which is two times as large as the impact velocity. This high velocity ejection phenomenon is usually observed in crater formation just after the collision and is known as the jetting process. After 80 μs, movement of the envelope at the rear side can be recognized. The ejection velocity at the rear is lower than the jetting velocity. The measured velocity is about 70 m s^{-1}, which is 20 times smaller than the jetting velocity. From being initially round, the envelope at the rear side gradually deforms to a horizontal straight line with time. The deformation clearly shows that the fragment velocity becomes larger with decreasing distance from the impact point.

The collisional energy of this study was so large for ice that almost all of the fragments fractured into pieces smaller than 5 mm except for Run 8. The largest fragment mass recovered after the collision was estimated to be smaller than 0.1 g according to a proposed scaling law on impact fragmentation of ice (Mizutani *et al.*, 1990; Kato *et al.*, 1995). Because fragments smaller than 1 mm cannot be resolved in a photograph owing to limited spatial resolution, we cannot identify most of the fragments individually. Thus, we can only observe the envelope made of these fragments including icy dust.

Figure 2 shows contours for the ejecta envelopes traced from the images in Fig. 1 and is used for analyzing the ejection velocities. An envelope of the black region in the recorded images was traced by hand. A labeled time means time relative to the first image. For measuring the velocity, the impact point is defined as the origin of a rectangular coordinate system indicated on the figure. In this coordinate system, the right horizontal axis is used as a base line from which an angle of the initial position of fragments (θ) was measured. The lower vertical axis is defined as $\theta = 90°$. We used the "radiant point model" proposed by Paolicchi *et al.* (1989) to analyze the ejection velocity because individual fragments cannot be detected separately in our images. According to this model, all the velocity vectors of ejected fragments radiate from one point called the "radiant point". Nakamura and Fujiwara (1991) showed that the radiant point obtained from their high velocity impact experiments ($\geqslant 3$ km s^{-1}) for rock with a small mass ratio ($m_p/M_t \leqslant 7 \times 10^{-4}$) was buried at a depth of 1/3–1/4 the target diameter beneath the impact point. Because there is no information on the radiant point depth for ice collisions, and because the present experimental conditions are very different from those of Nakamura and Fujiwara, a simple assumption is made in our analysis: the radiant point corresponds to the impact

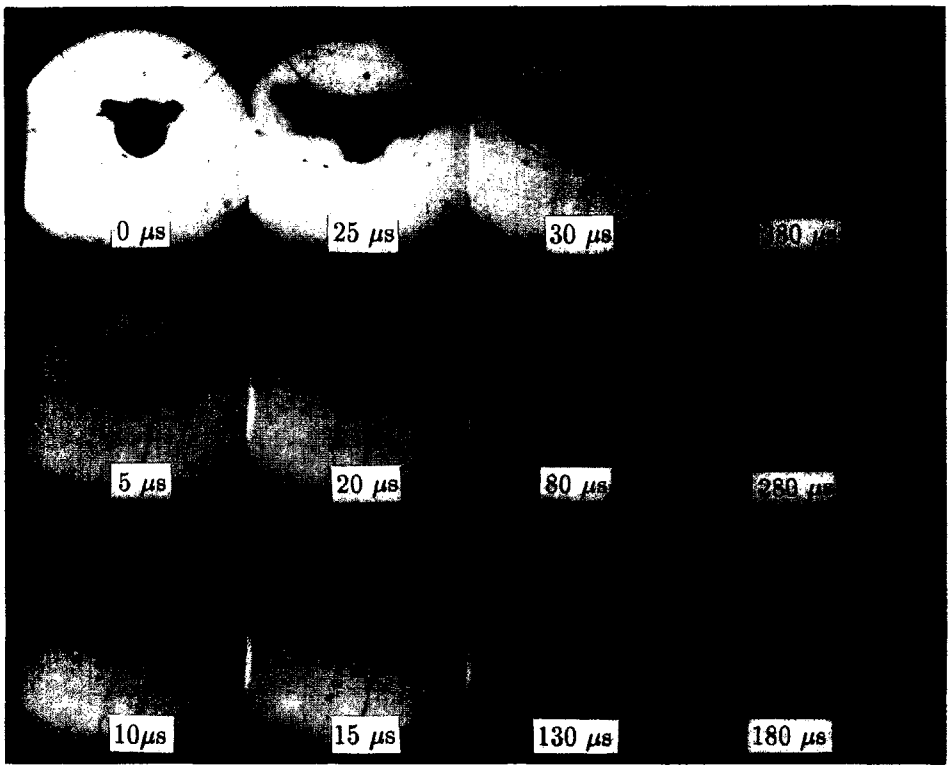

Fig. 1. Twelve successive images of collisional disruption in Run 6 taken by an image-converter camera. Frame speed of the camera changes from 2×10^5–2×10^4 frames s^{-1} at 8th image and 2×10^4 to 1×10^4 frames s^{-1} at 11th image

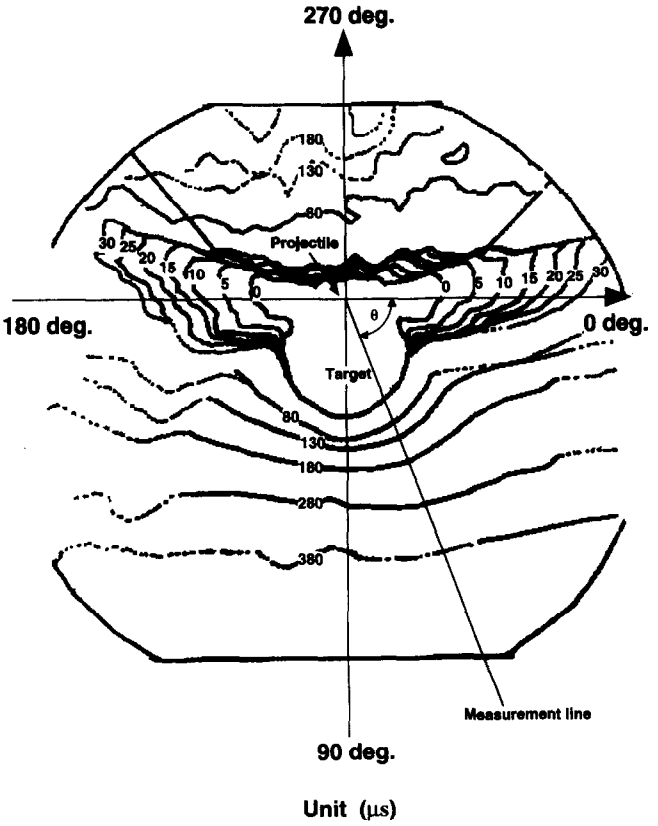

Fig. 2. Contours of ejecta envelopes traced from the images in Fig. 1. Numbers labeled on the contours are progress time (μs). Ejecta velocity was analyzed along a measurement line every 10° initial position angle (θ). An origin of rectangular coordinate system applied in this figure is set at an impact point

point of the two spheres. Thus the velocity of fragments on the surface of the target sphere can be obtained by measuring the envelope expansion on the measurement line. This ejection velocity was measured from 30° to 150° in 10° increments.

Ejection phenomenon near the impact point is closely related to the jetting process. The relation between impact velocity (V_i) and the jetting velocity (V_{jet}) normalized by the impact velocity is shown in Fig. 3. The broken line is the normalized jetting velocity (V_{jet}/V_i) of 1. All the data are higher than this line and scatter from 1.7 to 2.9, which means that the jetted ejecta always has velocity higher than the impact velocity. In this figure, the normalized jetting velocity does not seem to depend on the impact velocity and mass ratio.

The condition for jetting in the collisions of ice spheres was examined by McKinnon (1989). He showed that the jetting could occur during the impacts at relative velocities as low as $\sim$ 500 m s^{-1} as it was observed in our experiments. Vickery (1993) also developed a theory of the jetting process in collisions of a spherical projectile at variable angles on a half space target. Vickery calculated the jetting velocity and ejecta mass for various initial conditions to apply these results to the origin of tektites. Her theory and previous experiments apparently show that the normalized jetting velocity decreases with increasing impact velocity and gradually approaches a constant at higher impact velocity. For example, the normalized jetting velocity for dunite collision decreases from 18 at

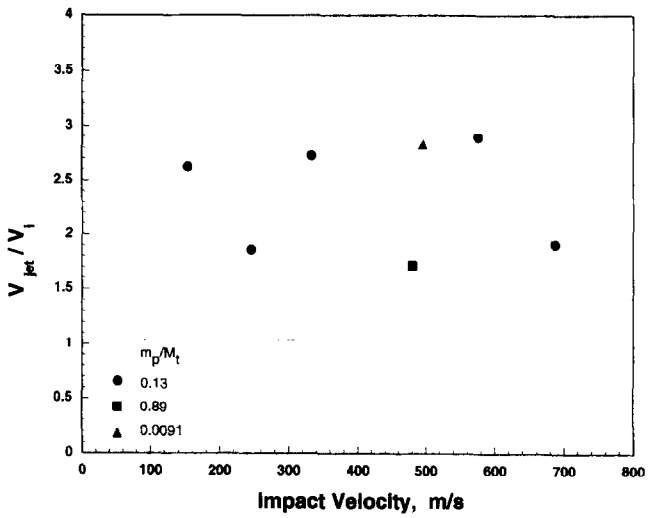

Fig. 3. Normalized jetting velocity at the impact of 150–690 m s^{-1}. The results in the three different mass ratios are compared (0.89, 0.13, 0.0091). The dashed line is $V_{jet}/V_i = 1$

an impact velocity of 3 km s^{-1} to a constant value of 3 at an impact velocity of 6 km s^{-1}. But our results for ice show that the normalized jetting velocity is almost constant for impact velocities between 150 and 690 m s^{-1}. A lower impact velocity may cause the decreasing trend of the normalized jetting velocity against impact velocity. Additional experiments, with a wider range of impact velocities, are needed to confirm the above speculation.

The ejection velocity at the antipodal point, which is the velocity in the direction of 90° (V_a), has been described by a scaling law for impact fragmentation by an appropriate parameter such as specific energy (Q) (Fujiwara and Tsukamoto, 1980):

$$Q = \frac{1}{2}\frac{m_p}{M_t} V_i^2.$$

Figure 4 shows the relation of the antipodal velocity as a

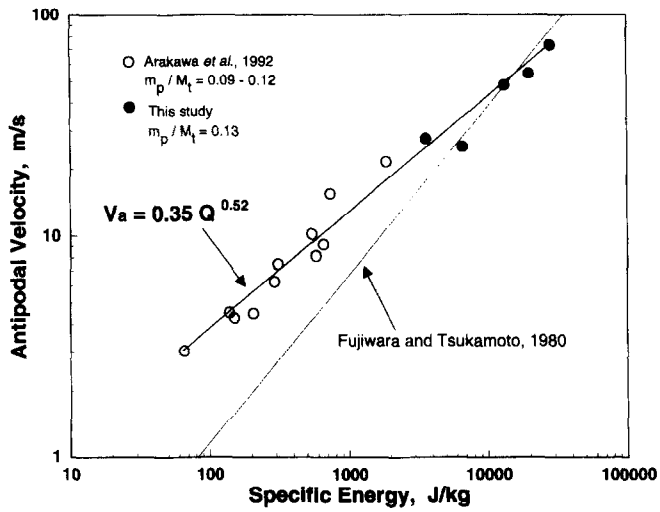

Fig. 4. Antipodal velocity vs. specific energy. The data of Arakawa *et al.* (1992) in low velocity collisions for ice are used for obtaining the empirical relation shown in equation (1). The data on basalt in Fujiwara and Tsukamoto (1980) is shown by a thin line for comparison

function of Q at a nearly constant mass ratio of about 0.1 including the data of Arakawa *et al.* (1992) from a low velocity collisional experiment on ice. We extended the relation between Q and V_a from 2×10^3 to 2×10^4 J kg^{-1} by using our new data at high velocity. All the data can be fit by the power law relation described as

$$V_a = 3.5\times10^{-1}Q^{0.52}. \quad (1)$$

$Q^{0.52} \sim Q^{0.5}$ and so $V_a \approx 7\times10^{-2}V_i$ for this mass ratio (0.1). This may be a simpler way to state the result, i.e. given fixed m_p/M_t antipodal velocity increases nearly linearly with impact velocity. The dependence of V_a on material is an important unresolved problem, so the V_a for basalt collision is compared with our results. Fujiwara and Tsukamoto (1980) measured the antipodal velocity for a basalt target colliding at $V_i = 2.7$ km s^{-1} and $m_p/M_t = 2.6\times10^{-2}$–$2.6\times10^{-4}$ and obtained a relation between V_a and Q described by $V_a = 3.2\times10^{-2}Q^{0.76}$. It is noted that V_a for ice is higher than for basalt for the specific energies lower than 2×10^4 J kg^{-1}. However, the difference between ice and basalt gradually decreases with increasing Q and at $Q = 2\times10^4$ J kg^{-1} they have almost the same value of V_a, even though ice and basalt have distinctly different physical properties. The slope of the data is different between ice and basalt impacts. This difference will be primarily caused by the target material properties, however the strain rate dependence of the material strength may affect the difference of slopes. Because the strain rate, which is controlled by the impact velocity and the target size, achieved in the samples for our impacts and Fujiwara and Tsukamoto would be distinctly different.

The velocity field of fragments ejected far from the impact point is shown in Fig. 5, where the vertical axis is the ejection velocity and the horizontal axis is the initial position angle (θ) as defined in Fig. 2. The antipodal point is at 90°. Results for three impact velocities at a mass ratio of 0.13 are shown. The velocity field for a collision at 687 m s^{-1} is almost symmetrical about the angle of 90°. The velocity has a minimum at the antipodal point and rapidly increases from 80 to 180 m s^{-1} away from the antipodal point. In the collisions at 575 and 470 m s^{-1}, the symmetry of the velocity field is slightly broken: the minimum velocity occurs at 100° for the impact at 470 m s^{-1} and 80° for the impact at 575 m s^{-1}. In these collisions, the projectile collided with the target obliquely at an incidence angle of several degrees; the oblique components of the impact may have caused the asymmetry in the observed velocity distribution. The ejection velocity at all initial positions increases with increasing impact velocity and the curves showing the velocity field become steeper in higher velocity collisions.

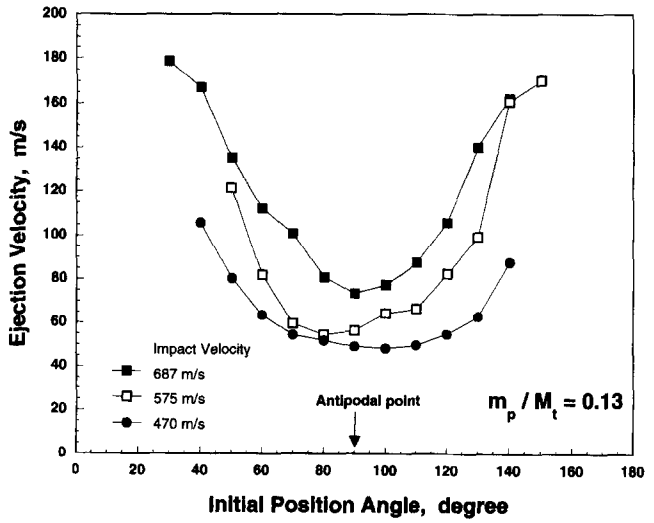

Fig. 5. Velocity field of the collisional ejecta at $30° \leqslant \theta \leqslant 150°$ for the impact velocity of 470, 575, and 687 m s^{-1}. The mass ratio is 0.13

Discussion

Figure 6 shows, for Run 6, a relation between the ejection velocity and the distance from the impact point to the initial fragment position (l) normalized by the target diameter (D). A value of 1 corresponds to the antipodal point. Because the velocity field was quite symmetric in this collision, the data for the initial positions between 40° and 140° can be fit by the following equation:

$$V_e = V_a\left(\frac{l}{D}\right)^{-n} \quad (2)$$

where n is 2.0. The exponent n varies with the impact velocity or possibly scatters due to experimental errors: it is 1.5 at 470 m s^{-1} and 2.0 at 575 m s^{-1}. The velocity field ($30° \leqslant \theta \leqslant 150°$) for ice collisions under any conditions within our experimental range can be estimated from equations (1) and (2). By substituting equation (1) into equation (2), V_e at any initial position is derived as

$$V_e = 0.24\left(\frac{m_p}{M_t}\right)^{0.52} V_i^{1.1}\left(\frac{l}{D}\right)^{-n} \quad (3)$$

but this is only the surface ejection velocity at best; more material below the surface will bring lower velocities. This equation will be used to determine the reaccumulation conditions for collisions among icy planetesimals.

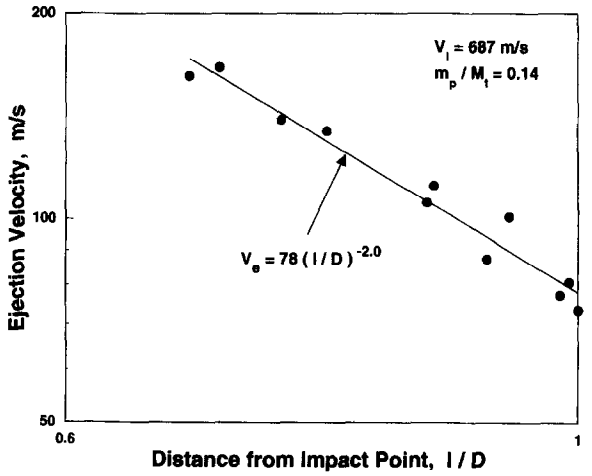

Fig. 6. Relation between the ejection velocity and the normalized distance from the impact point to the initial position at $40° \leqslant \theta \leqslant 140°$ in Run 6

Asphaug and Melosh (1993) used a numerical model to study the effect of a large impact on a small body of ice composition and showed how the surface ejection velocity varied with distance from the impact site. Their simulations resulted in an exponent n of about 1.6, a value similar to the result obtained by the observation of the underground explosions. This exponent corresponded to our result ranging from 1.5 to 2.0, although their impact condition was very different from ours: their model was calculated at $v_i = 1.5$ km s^{-1}, $m_p/M_t = 1.1 \times 10^{-5}$ and $Q = 12$ J kg^{-1}. We also compared the antipodal velocity calculated by using equation (3) at the impact condition of Asphaug and Melosh with the result of their simulation. Thus, $V_a = 1.2$ m s^{-1} was obtained and this velocity agreed well with that computed by Asphaug and Melosh (~ 1 m s^{-1}).

When we apply our experimental results to collisions at planetary scales, it is necessary to consider the attractive force of gravity among the fragments. Before gravitational potential energy is compared with fragment kinetic energy to determine the reaccumulation conditions of the fragments, our results must be transformed from the laboratory frame to a center of mass frame. Figure 7 shows the velocity field calculated by equation (3) in the center of mass frame at the collisional conditions of Run 6. The ejection velocity close to the antipodal point is almost 0 m s^{-1} and neighboring fragments are ejected horizontally with velocities below about 50 m s^{-1}. The horizontal velocity component is always larger than the vertical component parallel to the impact direction at all initial positions ($30° \leqslant \theta \leqslant 150°$). The vertical velocity component becomes smaller as the antipodal point is approached, thus the fragments are ejected almost normal to the impact direction.

The reaccumulation conditions for fragments from head-on collisions of icy planetesimals at 500 m s^{-1} and a mass ratio of 0.13 are shown in Fig. 8, where the vertical axis is the ejection velocity in the center of mass frame and the horizontal axis is the initial position angle of the fragments. Icy planets with a density of 1000 kg m^{-3} are

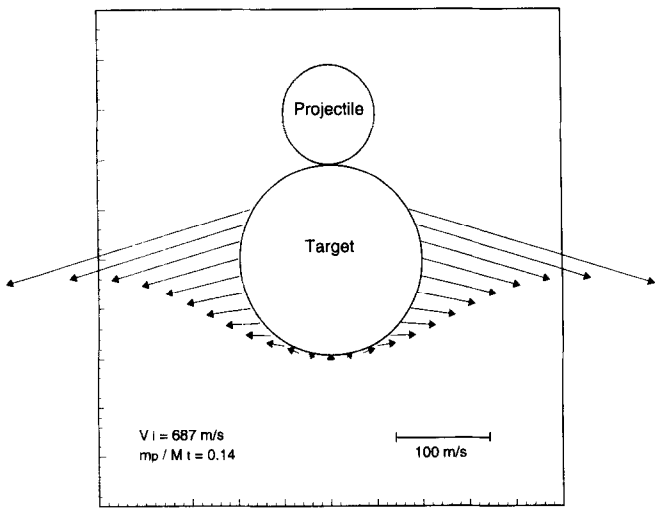

Fig. 7. Velocity vectors of the collisional ejecta at $30° \leqslant \theta \leqslant 150°$ in center of mass frame (Run 6). Velocity of the center of mass is 81 m s^{-1}

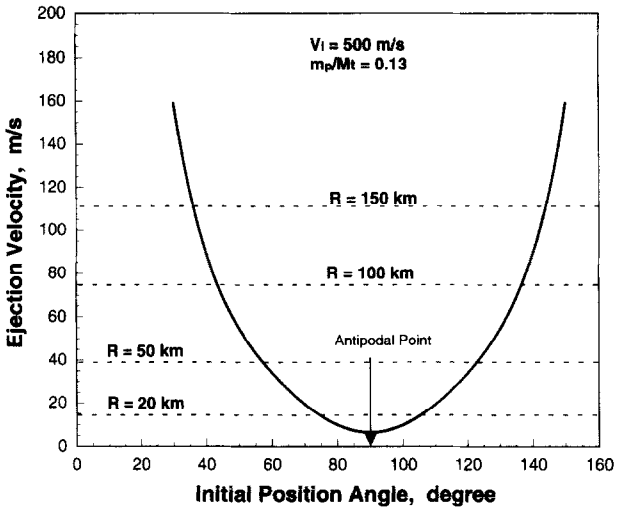

Fig. 8. Reaccumulation conditions of ejecta far from the impact point ($30° \leqslant \theta \leqslant 150°$) in the collision of $V_i = 500$ m s^{-1} and $m_p/M_t = 0.13$. R is the radius of the icy planets with the density of 1000 kg m^{-3} and the dashed lines show the escape velocity of these planets. The ejecta with the velocity lower than the dashed line can accumulate on the parent planet through its self gravity

assumed in this computation. The escape velocity of these bodies varies from 15 to 112 m s^{-1} as the body radius changes from 20 to 150 km. This size-dependent escape velocity of each planet is compared with the velocity distribution estimated from equation (3) in the center of mass frame. As a result, in this collision, the bodies smaller than 20 km cannot recapture fragments except for those near the antipodal point. On the other hand, bodies larger than 100 km can capture fragments from a wider range of initial positions between 40° and 140°. Here they will grow effectively by reaccumulation after collisional disruption. We cannot discuss the quantity of reaccumulating mass because the velocity field obtained was only for the fragments coming from the target surface and because the mass of each fragment was not measured. For a more quantitative discussion of the growth process of the icy planetesimals, we need to determine the mass and the velocity of each ice fragment in detail.

We have some of the scaling problems to extrapolate from small experiments to kilometer-size bodies in Fig. 8. Large-scale events, such as a collision with an icy satellite, involve much lower strain rates than do typical small-scale laboratory tests, thus the effective strength of large targets will be considerably smaller than those used in our experiments. Collisional outcomes also depend on large target size because, for bodies larger than a few kilometers, gravitational forces effectively increase the target strength. Thus, these problems must be noted in the application of our results to the reaccumulation of fragmented satellites.

Acknowledgements. We greatly thank Prof. N. Maeno of the Institute of Low Temperature Science, Hokkaido University and Dr S. Watanabe of the Department of Earth and Planetary Science, Nagoya University, for their useful discussions on the experiment, and Drs Y. Iijima and M. Kato of the Department of Earth and Planetary Science, Nagoya University and N. Onose of the Institute of Low Temperature Science, Hokkaido University, for their help in constructing the experimental apparatus and performing the experiment. We also thank S.

Nakatsubo and T. Segawa of the Contribution Division of Institute of Low Temperature Science, Hokkaido University for their technical help to the experiment. We acknowledge Prof. H. J. Melosh of the Lunar and Planetary Lab., University of Arizona for his useful advice to improve our manuscript.

References

Arakawa, M., Higa, M., Maeno, N., Iijima, Y., Okimura, Y., Kato, M., Fujimura, A. and Mizutani, H., Measurements of fragment velocities in ice–ice collisions, in *Abstracts of Japanese Earth and Planetary Science Joint Meeting*, p. 441, 1992.

Asphaug, E. and Melosh, H. J., The stickney impact of Phobos: a dynamical model. *Icarus* **101,** 144–164, 1993.

Benz, W. and Asphaug, E., Impact simulations with fracture. 1. Method and tests. *Icarus* **107,** 98–116, 1994.

Frisch, W., Hypervelocity impact experiments with water ice targets, in *Proceedings of the Workshop on Hypervelocity Impacts in Space* (edited by J. A. M. McDonnell), pp. 7–14, University of Kent, Canterbury, 1991.

Fujiwara, A. and Tsukamoto, A., Experimental study on the velocity of fragments in collisional breakup. *Icarus* **44,** 142–153, 1980.

Giblin, I., Martelli, G., Smith, P. N., Cellino, A., Di Martino, M., Zappala, V., Farinella, P. and Paolicchi, P., Field fragmentation of macroscopic targets simulating asteroidal catastrophic collisions. *Icarus* **110,** 203–224, 1994.

Kato, M., Iijima, Y., Arakawa, M., Okimura, Y., Fujimura, A., Maeno, N. and Mizutani, H., Ice-on-ice impact experiments. *Icarus* **113,** 423–441, 1995.

McKinnon, W. B., Impact jetting of water ice, with application to the accretion of icy planetesimals and Pluto. *Geophys. Res. Lett.* **16,** 1237–1240, 1989.

Mizutani, H., Takagi, Y. and Kawakami, S., New scaling laws on impact fragmentation. *Icarus* **87,** 307–326, 1990.

Nakamura, A. and Fujiwara, A., Velocity distribution of fragments formed in a simulated collisional disruption. *Icarus* **92,** 132–146, 1991.

Paolicchi, P., Cellino, A., Farinella, P. and Zappala, V., A semi-empirical model of catastrophic breakup processes. *Icarus* **77,** 187–212, 1989.

Vickery, A. N., The theory of jetting: application to the origin of tektites. *Icarus* **105,** 441–453, 1993.